Vehicle System Dynamics: International Journal of Vehicle Mechanics and Mobility

Publication details, including instructions for authors and subscription information:
http://www.tandfonline.com/loi/nvsd20

Torque blending and wheel slip control in EVs with in-wheel motors

Ricardo de Castro [a], Rui E. Araújo [a], Mara Tanelli [b], Sergio M. Savaresi [b] & Diamantino Freitas [a]

[a] Faculdade de Engenharia da Universidade do Porto, Rua Dr. Roberto Frias, s/n, 4200-465, Porto, Portugal

[b] Dipartimento di Elettronica e Informazione, Politecnico di Milano, Piazza L. Da Vinci, 32, 20133, Milan, Italy

Version of record first published: 16 Jul 2012.

To cite this article: Ricardo de Castro , Rui E. Araújo , Mara Tanelli , Sergio M. Savaresi & Diamantino Freitas (2012): Torque blending and wheel slip control in EVs with in-wheel motors, Vehicle System Dynamics: International Journal of Vehicle Mechanics and Mobility, 50:sup1, 71-94

To link to this article: http://dx.doi.org/10.1080/00423114.2012.666357

Vehicle System Dynamics
Vol. 50, Supplement, 2012, 71–94

Torque blending and wheel slip control in EVs with in-wheel motors

Ricardo de Castro[a]*, Rui E. Araújo[a], Mara Tanelli[b], Sergio M. Savaresi[b] and Diamantino Freitas[a]

[a]*Faculdade de Engenharia da Universidade do Porto, Rua Dr. Roberto Frias, s/n, 4200-465 Porto, Portugal;* [b]*Dipartimento di Elettronica e Informazione, Politecnico di Milano, Piazza L. Da Vinci, 32, 20133 Milan, Italy*

(*Received 24 October 2011; final version received 6 February 2012*)

Among the many opportunities offered by electric vehicles (EVs), the design of power trains based on in-wheel electric motors represents, from the vehicle dynamics point of view, a very attractive prospect, mainly due to the torque-vectoring capabilities. However, this distributed propulsion also poses some practical challenges, owing to the constraints arising from motor installation in a confined space, to the increased unsprung mass weight and to the integration of the electric motor with the friction brakes. This last issue is the main theme of this work, which, in particular, focuses on the design of the anti-lock braking system (ABS). The proposed structure for the ABS is composed of a tyre slip controller, a wheel torque allocator and a braking supervisor. To address the slip regulation problem, an adaptive controller is devised, offering robustness to uncertainties in the tyre–road friction and featuring a gain-scheduling mechanism based on the vehicle velocity. Further, an optimisation framework is employed in the torque allocator to determine the optimal split between electric and friction brake torque based on energy performance metrics, actuator constraints and different actuators bandwidth. Finally, based on the EV working condition, the priorities of this allocation scheme are adapted by the braking supervisor unit. Simulation results obtained with the CarSim vehicle model, demonstrate the effectiveness of the overall approach.

Keywords: electric vehicles; brake-by-wire; adaptive control; ABS; braking system

1. Introduction

Electric vehicles (EVs) and hybrid EVs represent a promising alternative to the traditional internal combustion-based vehicles, and are receiving increasing support from the automotive industry, academy, governments and the general public. The driving force behind this paradigm shift is being encouraged by the environmental benefits, like reduction in pollutant emissions and a decrease in the consumption of fossil resources [1]. From an engineering perspective, these new energy sources demand a redesign of the power train control in order to accommodate a new type of actuator: the electric motor. The advantages of this new actuator are well known,

*Corresponding author. Email: de.castro@fe.up.pt

ISSN 0042-3114 print/ISSN 1744-5159 online

http://dx.doi.org/10.1080/00423114.2012.666357
http://www.tandfonline.com

and can be summarised in three main factors [2–4]: (i) regenerative braking, (ii) fast and accurate torque control, (iii) the possibility, if a multi-motor configuration is employed, to independently regulate the torque (accelerating or braking) transmitted to each driven wheel. The first factor gives an important contribution to increase the vehicle energy efficiency [5], while the latter features can be exploited to improve the performance of active safety systems, like traction control [2], and to actively modify the vehicle handling and yaw response [3,4,6].

This work deals with anti-lock braking systems (ABS) design for EVs in which the power train does not contain a mechanical differential and the accelerating/braking torque transmitted to each driven wheel can be individually regulated. Such class of power trains can be found on vehicles with in-wheel electric motors [2,3,7] or with more simple solutions based on traditional electric motors coupled to the wheel through belts [6] or single-gear transmissions [8]. As a result, the ABS employed in these vehicles can be classified according to the type and number of actuators, thus we can have ABS based on: (i) electric motor, (ii) friction brakes and (iii) combined/hybrid actuation (electric motor and friction brakes). From the control and energy efficiency point of view, the first approach, where the ABS solely relies on the electric motor [3,8], is sound, but suffers from some practical limitations; for instance, the torque generated by the electric motor is severely reduced when the motor operates in the field weakening region or when the energy source is approaching the full charge state. Consequently, in these situations, the vehicle's braking ability is compromised, as well as the ABS functionality. From the robustness and reliability perspective, disabling the electric motor during the ABS and employing the traditional friction brakes, like hydraulic or electro-hydraulic [9], is the most simple approach to the ABS design [6]. The main motivation for the latter approach is due to the fact that, during emergency braking situations, the regenerative property of the electric motor is not a top priority (the vehicle safety has precedence), so the electric motor can be safely disabled. However, this argument overlooks one important feature in the electric actuator: the fast torque response. As pointed out in Figure 1, the electric motor should be regarded as a braking device, which, although having a limited actuation authority, extends the bandwidth of the previous generations of friction brakes. Hence, to take full advantage of all the capabilities available in the braking devices, the most interesting configuration is the one where the electric motor and the friction brakes are simultaneously controlled by the ABS, which is named hybrid ABS in the present article. It should be noticed that the cooperation between the electric motor and friction brakes, during 'normal braking' manoeuvres (i.e. when small values of wheel slip occur), was the subject of several works in recent years (see [5,10] and references therein). However, these studies are usually focused on maximising the energy efficiency during the 'normal braking' situations, and do not take into account the torque-sharing strategies suitable for the ABS operation. Furthermore, the control of hybrid

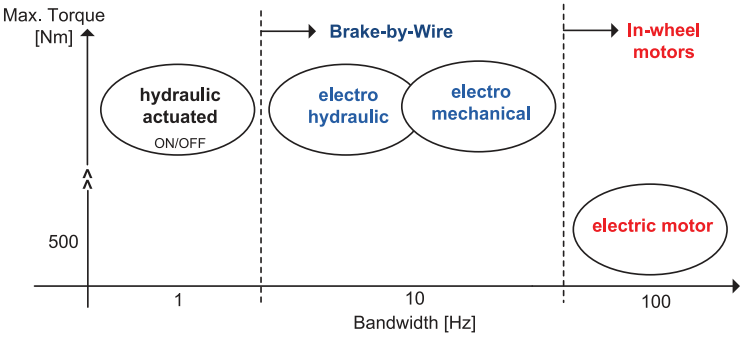

Figure 1. Qualitative features of the braking devices in the EVs.

ABS configurations has received little attention in the literature. In the automotive industry, we can find some hybrid ABS application examples, most notably the prototypes of Toyota with in-wheel motors [2], but these manufacturers, understandably, are not willing to disclose all the details of the control system.

The main objective of this work is to design a new control strategy for the hybrid ABS, capable of complementing the friction brakes with the quick, but limited, regenerative torque offered by the electric motor. To this aim, we propose a decoupled structure based on two layers. The first layer addresses the tyre slip regulation problem using a robust adaptive controller, able to cope with the parametric uncertainty in the tyre–road friction and other non-parametric disturbances. In the second layer, a torque allocator is responsible for distributing the torque requested by the ABS among the two braking devices, taking into consideration the actuators limitations, that is, torque range, rate limit and nonlinear constraints (e.g. field weakening in the electric motor), and performance metrics, such as energy efficiency and braking actuation bandwidth. This distribution is performed by a control allocation (CA) approach [11,12] and is formulated as an optimisation problem, solved using an efficient numeric solver, suitable for realtime implementation. With this design approach, we can decouple the slip regulation problem and the torque allocation one, and benefit from the full capabilities of the braking devices.

2. Overview of the braking system

Generally, the braking system has the responsibility of safely decelerating the car in accordance with the braking force requested by the driver (F_x in Figure 2). The first step to achieve this goal consists of defining the amount of force that the front and rear axles will produce (Figure 2). Historically, this distribution has been designed having in mind that, from the vehicle stability point of view, the rear wheels should never lockup before the front ones [13]. Consequently, optimal front–rear distributions can be devised in order to ensure the simultaneous locking of both axles, as discussed in [13]. After defining the front–rear distribution, the individual braking forces for each wheel are generated by adding/subtracting the differential braking signals required by the vehicle dynamics controller (e.g. the yaw-rate and/or side-slip controllers [14,15]). A more recent trend, spurred by the increasing amount of actuation available in modern vehicles, is to bypass the front–rear distribution and use the vehicle dynamics controller to generate the references for the individual (longitudinal and lateral) wheel forces, taking into

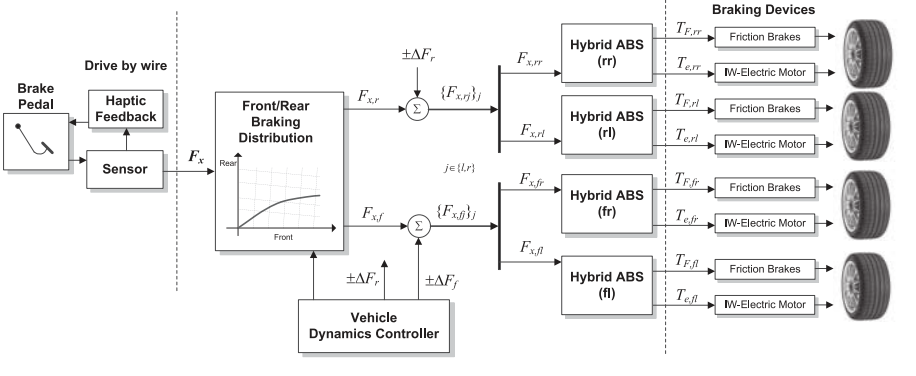

Figure 2. Generic architecture of the EV braking system with in-wheel electric motors and friction brakes; ΔF_{f} and ΔF_{r} represent differential braking signals and $F_{x,\mathrm{fl}}, F_{x,\mathrm{fr}}, F_{x,\mathrm{rl}}$ and $F_{x,\mathrm{rr}}$ are the desired braking forces for each wheel.

account the requested forces, yaw moments and tyre constraints [16,17]. In this work, it is assumed that the longitudinal force reference for each wheel is available, for example, using one of the above methods, and our interest lies on the hybrid ABS problem, with particular emphasis on the following issues: (i) understand how the longitudinal wheel force (or torque) should be distributed among the two braking devices and (ii) ensure that, when a large wheel torque is applied, the tyre slip is regulated to a safe value.

2.1. *Braking devices: control-oriented models and constraints*

According to the hybrid braking configuration presented in Section 1, assume that each wheel is equipped with two braking devices: friction brakes and in-wheel motor (IWM). In both cases, the braking torque response can be approximated as a first-order system with delay:

$$\frac{T_i}{T_i^*}(s) = \frac{1}{\tau_i s + 1}\,\mathrm{e}^{-\delta_i s}, \tag{1}$$

where T_i^* is the reference torque, T_i the output torque, τ_i the dominant time constant, δ_i the pure delay and $i \in \{f, e\}$ ($e =$ electric, $f =$ friction). For the friction brakes, this continuous torque regulation can be accomplished by employing electro-hydraulic or electro-mechanic brakes, as discussed in [9]. On the other hand, the IWM provides, in general, a much faster torque response [18], but the maximum torque is limited by two main factors: maximum regenerative power and battery state of charge (SoC). The first issue is related with the limited power (when compared with the friction brakes) that motor can regenerate, which restricts the braking torque in the high-speed zone. The second factor is the battery SoC: when the full charge condition is reached, the energy regeneration is no longer possible, which severely compromises the IWM braking torque. Thus, unlike the friction brakes, the maximum regenerative torque in IWM depends both on the wheel speed and battery SoC, thus yielding

$$T_{\mathrm{e,max}}(v, I_{q,\max}, \omega) = p(v)(1 - I_{q,\max}) \begin{cases} T_{\mathrm{e,n}}, & \omega \le \omega_{\mathrm{n}}, \\ T_{\mathrm{e,n}} \dfrac{\omega_{\mathrm{n}}}{\omega}, & \omega > \omega_{\mathrm{n}}, \end{cases} \tag{2}$$

where $I_{q,\max} \in \{0, 1\}$ is an indicator for the full SoC condition, $T_{\mathrm{e,n}}$ the peak braking torque and ω_{n} the motor nominal speed. The second branch in the above relation is due to the torque limitation introduced when the electric motor is operating in the constant power zone (also known as the field-weakening region in the electric drives field [19]), while $p(v)$ aims at disabling the regenerative braking when the vehicle is approaching the full stop; in this work, a simple sigmoid function

$$p(v) = \frac{1}{1 + \mathrm{e}^{-k_v(v - v_0)}} \tag{3}$$

is used to model this mechanism, where k_v and v_0 are tuning factors that define the speed zone and rate at which the electric motor is taken out of service.

Generally, both braking devices must also comply with range and rate limits:

$$T_{i,\min} \le T_i \le T_{i,\max}, \quad -\dot{T}_{i,\max} \le \dot{T}_i \le \dot{T}_{i,\max}, \quad i \in \{e,f\}, \tag{4}$$

where $T_{i,\min}, T_{i,\max}$ (N m) represent the braking torque range and $\dot{T}_{i,\max}$ (N m/s) the maximum rate limit (assumed symmetrical). In the case of frictional brakes, the minimum torque is zero ($T_{\mathrm{f,min}} = 0\,\mathrm{N\,m}$), the maximum $T_{\mathrm{f,max}}$ is normally very high and the rate limits may appear as a consequence of physical constraints on the variation rate at which the actuator

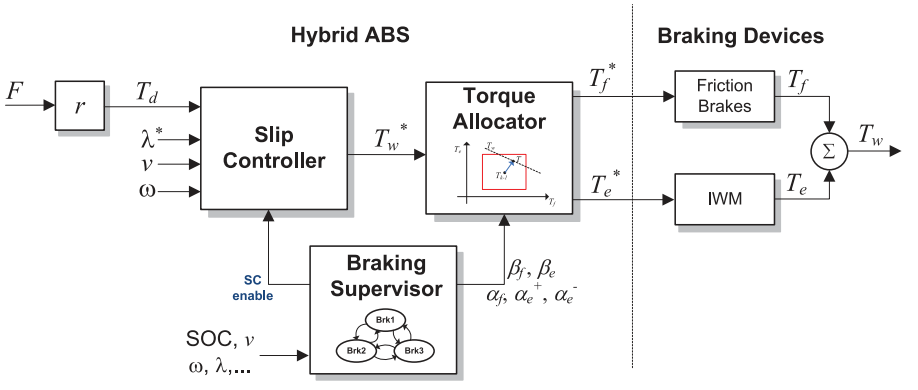

Figure 3. Block diagram of the proposed hybrid ABS structure.

change the pressure/force. As for the IWM, the highest regenerative torque $T_{\mathrm{e,max}}$ was already discussed in Equation (2), while the minimum (acceleration) torque is given by $T_{\mathrm{e,min}} = -T_{\mathrm{e,max}}(v, I_{q,\mathrm{min}}, \omega)$, with $I_{q,\mathrm{min}}$ representing a minimum SoC flag; the rate limit in this actuator is related with current rate constraints at which the EV batteries can be charged [20].

2.2. *Hybrid ABS*

Hereafter, we concentrate on the design of the hybrid ABS, which is composed by three modules: (i) slip controller (SC), (ii) torque allocator and (iii) a braking supervisor. As can be seen in Figure 3, there is a clear separation between the slip regulation task and the torque allocation, which was adopted with the aim of simplifying the control problem. For example, with this modular approach, the design of the slip regulator can focus on the stability and robustness issues, for example, due to friction variations and other disturbances, and only need to generate the desired wheel torque (T_{w}^*). On the other hand, the complexity associated with the split between electric/friction torque is deferred to a second block, the torque allocator, which handles the actuators range and rate limit constraints, energy performance metrics, different bandwidths, etc. This separation also allows the application of different tools to independently solve each of the above tasks, that is, the stability and robustness issues can be addressed with Lyapunov-based techniques, while numerical optimisation techniques are more appropriated to deal with the allocation problem (due to the multi-objective nature of this second task). As an added bonus, the torque allocator can also be used during normal braking manoeuvres. Finally, a braking supervisor is incorporated in the hybrid ABS in order to manage the different modes in which the torque allocator can operate, and, whenever necessary, enable/disable the SC. The next three sections will be devoted to the description and discussion of the three elements that compose the hybrid ABS.

3. Slip controller

We will start the presentation of the hybrid ABS by tackling the problem of wheel slip control. Given that the braking actuators are (directly or indirectly) torque-controlled, it is convenient to first translate the desired longitudinal force for the tyre (F), generated by the hierarchical approach discussed in the previous section, in a 'desired' wheel torque $T_{\mathrm{d}} = F/r$, where r is the wheel radius (Figure 3). To simplify the controller design, the actuators dynamics can be

neglected and considered in the validation phase. Whereas the validity of this approximation is more than reasonable for the fast IWM, the delays present in the friction brakes actuator may raise some concerns. Nevertheless, as our ultimate goal is to blend the torque produced by both actuators, it will be shown that by a careful design of the torque allocator block, the above assumption holds (e.g. by making the IWM respond to the high frequency content of the wheel torque).

3.1. *Quarter car model*

As a starting point for the design of the SC, the quarter car model (QCM) [3,9,21] is used to represent the vehicle longitudinal motion:

$$M\dot{v} = -F_z\mu(\lambda) - \Delta_v(t, v), \tag{5a}$$

$$J\dot{\omega} = rF_z\mu(\lambda) - T_{\mathrm{w}} - \Delta_w(t, \omega), \tag{5b}$$

$$\lambda = h(v, \omega) = \frac{v - \omega r}{v}, \tag{5c}$$

where $(v, \omega) \in \mathcal{D}$ are the system states, composed by the vehicle velocity v and the wheel speed ω, the braking torque T_{w} is the input and the tyre slip $\lambda \in \Lambda$ the output. The above model, valid in the (braking) domain $\mathcal{D} = (0, \infty) \times [0, \infty) \subset \mathbb{R}^2$, depends on the following parameters: wheel inertia (J), quarter car mass (M), wheel radius (r) and wheel vertical load (F_z). The function $\mu(\lambda)$ represents the nonlinear friction coefficient in the tyre–road interface, which is uncertain, and the terms $\Delta_v(t, v)$ and $\Delta_\omega(t, \omega)$ are force and torque disturbances resulting from unmodelled dynamics. For instance, the disturbance Δ_v can be described, in its simplest form, by a polynomial $\Delta_v(t, v) = a_1 + a_2 v + a_3 v^2$ to account for the total resistance to the vehicle motion, arising from aerodynamic drag, rolling resistance and grade force [13]. In this work, it will be assumed that both disturbances are uniformly bounded:

$$|\Delta_v(t, v)| \leq \overline{\Delta_v}, \quad |\Delta_\omega(t, \omega)| \leq \overline{\Delta_\omega}, \quad \forall (t, v, \omega) \in [0, \infty) \times \mathcal{D}, \tag{6}$$

where $\overline{\Delta_v}$ and $\overline{\Delta_\omega}$ are known constants.

The control objective is to design a state feedback control law that will bring, as fast as possible, the system output λ to a given set point λ^*. Due to the nonlinear nature of the QCM (5), we will start by employing the concept of input–output (IO) linearisation [22] and computing the relative degree of the system. The first time derivative of the output has the form:

$$\dot{\lambda} = \frac{\partial h}{\partial v}\dot{v} + \frac{\partial h}{\partial \omega}\dot{\omega} \tag{7a}$$

$$= -\frac{r\omega}{v^2}\left(\frac{F_z\mu(\lambda) + \Delta_v(t, v)}{M}\right) - \frac{r}{v}\left(\frac{rF_z\mu(\lambda) - T_{\mathrm{w}} - \Delta_w(t, \omega)}{J}\right)$$

$$= -\frac{r/J}{v}\left(\left(1 + (1 - \lambda)\frac{J}{Mr^2}\right) r\mu(\lambda)F_z - T_{\mathrm{w}} - \Delta_\omega(t, \omega) + (1 - \lambda)\frac{J}{Mr^2} r\Delta_v(t, v))\right). \tag{7b}$$

Thus, defining the terms

$$p_1 = \frac{r}{J}, \quad p_2 = \frac{J}{Mr^2}, \quad \Psi(\lambda) = (1 + (1 - \lambda)p_2)r\mu(\lambda)F_z, \tag{8}$$

the slip dynamics can be described as

$$\dot{\lambda} = -\frac{p_1}{v}(\Psi(\lambda) - T_{\mathrm{w}} - \Delta_\omega(t,\omega) + (1-\lambda)p_2 r\Delta_v(t,v)), \tag{9}$$

which allows us to conclude that the system has a relative degree one for any $(v,\omega) \in \mathcal{D}$. In order to derive an ideal control law, suppose, for a moment, that $\Psi(\lambda)$ is known and the disturbances can be neglected ($\Delta_v = \Delta_\omega = 0$). Based on these (very unlikely) assumptions, letting the braking torque to be $T_{\mathrm{w}} = \Psi(\lambda) - vk(\lambda - \lambda^*)$, where $k > 0$ is a constant, yields

$$\dot{\lambda} = -p_1 k(\lambda - \lambda^*), \tag{10}$$

that is, a first-order slip response with exponential convergence to λ^*. This simple control law, although fulfilling the control objectives, requires the knowledge of the $\Psi(\lambda)$ function, which is difficult to ensure, given the uncertainties in the tyre–road friction $\mu(\lambda)$. Spurred by this difficulty, we will derive a robust adaptive method to handle the (parametric) uncertainty in $\Psi(\lambda)$ and cope, also, with the disturbances Δ_ω and Δ_v. Before describing the control law, a parametric representation for the Ψ function will be first outlined.

3.2. *Approximation of $\Psi(\lambda)$ with a linear parameterisation*

In view of the fact that $Mr^2 \gg J$ (and thus p_2 in Equation (8) is much smaller than 1), the function $\Psi(\lambda)$ can be rewritten as

$$\Psi(\lambda) = rF_z\mu(\lambda) + \Delta_{\Psi 1}(t,\lambda), \quad \Delta_{\Psi 1}(t,\lambda) = (1-\lambda)p_2 r\mu(\lambda)F_z, \tag{11}$$

where $\Delta_{\Psi 1}$ is a uniformly bounded disturbance, that is,

$$\begin{aligned} |\Delta_{\Psi 1}(t,\lambda)| &\le |(1-\lambda)|p_2 r\mu(\lambda)F_z \\ &\le p_2 r\mu_{\max}\overline{F_z} \le p_2 r\overline{\Delta_{\Psi 1}} \quad \forall (t,\lambda) \in [0,\infty) \times \Lambda \end{aligned} \tag{12}$$

with $\mu_{\max} = \max_\lambda \mu(\lambda)$, $\overline{F_z} = \max_t F_z(t)$ and $\overline{\Delta_{\Psi 1}} \ge \mu_{\max}\overline{F_z}$ a known constant. Notice that to establish the previous inequalities, we employed the fact that, during a braking manoeuvre, $0 \le r\omega \le v$, which together with the definition of λ in Equation (5c) restricts the slip domain to $\Lambda = [0,1]$. In practice, the above bound $\mu_{\max}$ can be obtained considering the highest possible grip in the tyre–road interface, while for $\overline{F_z}$, we can resort to well-known relations of the front–rear load transfer and extract the maximum feasible vertical load that the tyre may experience during a braking manoeuvre [23]. Joining these two bounds, $\overline{\Delta_{\Psi 1}}$ can be seen as an upper bound for the maximum value of the longitudinal force produced by the tyre.

Continuing with the analysis of $\Psi(\lambda)$, rewritten as in Equation (11), the main source of parametric uncertainty is in the friction coefficient $\mu(\lambda)$. For control design purposes, the tyre–road adhesion $\mu(\lambda)$ will be modelled as [24]

$$\mu(\lambda) = c_1 + c_2\lambda + c_3\,\mathrm{e}^{-c_4\lambda}, \tag{13}$$

where $c_i, i = 1,\ldots,4$ are the parameters of the Burckhardt model, not known *a priori* and time-varying with the adhesion and tyre operation conditions. As we intend to build adaptive mechanisms to deal with the QCM parametric uncertainty, it is convenient to represent $\mu(\lambda)$ as a linear parameterisation (LP). To this aim, notice that the first two terms in Equation (13) are already linear in the parameters, while the nonlinearity is confined to the last term. Given that, for the most representative types of road surfaces, the parameter $c_4 \in \mathcal{C} = [4,100]$ [24],

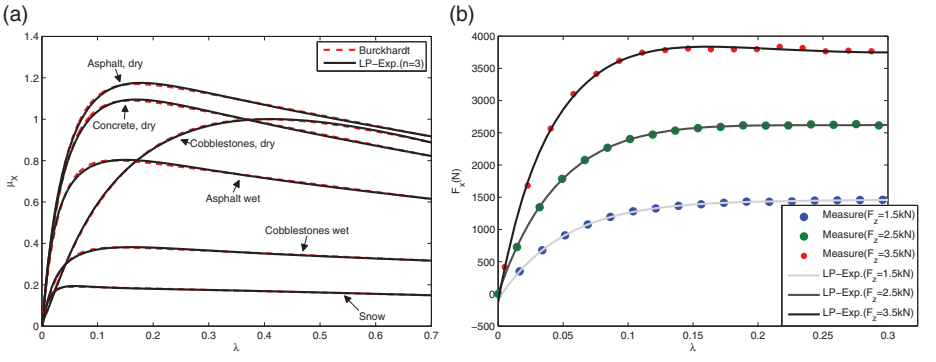

Figure 4. Fitting performance of Equation (16) when used to approximate: (a) the most common types of road surfaces predicted by the Burckhardt model [24], and (b) the experimental data of the longitudinal force produced by a 205/55 R16 90 H tyre [26].

the exponential term can be approximated as a sum of 'fixed' exponentials, appropriately weighted, that is, $e^{-c_4\lambda} \simeq \sum_{j=1}^{N} \theta_j e^{-w_j\lambda}$, where θ_j represent the linear parameters and w_j are fixed weights. In this approach, one natural question that arises is how many fixed exponentials (or basis functions in the function approximation terminology) should be employed in the approximation, which is then coupled with the second question on how to determine the w_j. As discussed in [25], the Burckhardt model, for $c_4 \in \mathcal{C}$, can be accurately approximated by the following LP:

$$\mu(\lambda) = \boldsymbol{p}^{\mathrm{T}}\Phi(\lambda)^{\mathrm{T}} + \Delta_\mu(\lambda), \quad |\Delta_\mu(\lambda)| \leq \overline{\Delta_\mu} \quad \forall\lambda \in \Lambda, \tag{14}$$

$$\boldsymbol{\Phi}(\lambda) = [1 \ \lambda \ e^{-4.99\lambda} \ e^{-18.43\lambda} \ e^{-65.62\lambda}]^{\mathrm{T}}, \tag{15}$$

where $\boldsymbol{p} \in \mathbb{R}^5$ is the set of linear parameters, $\boldsymbol{\Phi}(\lambda)$ is the (known) regressor and $\Delta_\mu(.)$ the approximation error introduced by the LP, bounded by a known constant $\overline{\Delta_\mu}$. To illustrate the approximation capabilities of this LP, Figure 4 presents the fitting offered by Equation (14) for the most representative types of road surfaces discussed in [24] and the experimental longitudinal force retrieved from [26]. In both cases, the performance is very satisfactory and the fitting errors almost negligible.

Finally, incorporating the LP approximation into Equation (11), one may express $\Psi(\lambda)$ as

$$\Psi(\lambda) = \boldsymbol{\theta}^{\mathrm{T}}\boldsymbol{\Phi}(\lambda) + \Delta_{\Psi 1}(t,\lambda) + \Delta_{\Psi 2}(t,\lambda), \tag{16}$$

where $\boldsymbol{\theta} = rF_z\boldsymbol{p} \in \mathbb{R}^5$ is a set of linear parameters (recall that r and F_z represent scaling factors and can be incorporated into the parameter $\boldsymbol{\theta}$) and $\Delta_{\Psi 2}(t,\lambda) = rF_z\Delta_\mu(\lambda)$ is a disturbance uniformly bounded by a known constant $\overline{\Delta_{\Psi 2}}$, that is,

$$|\Delta_{\Psi 2}(t,\lambda)| \leq |rF_z\Delta_\mu(\lambda)| \leq r\overline{F_z}\,\overline{\Delta_\mu} \leq \overline{\Delta_{\Psi 2}} \quad \forall(t,\lambda) \in [0,\infty) \times \Lambda. \tag{17}$$

3.3. *Robust adaptive slip control*

After presenting the system model, we now discuss a robust adaptive method to design the SC. To this aim, consider the regulation error

$$e = \lambda - \lambda^* \tag{18}$$

and redefine the control objective as the problem of finding the wheel torque T_{w} such that e converges to zero as fast as possible, in spite of uncertainties in Ψ and other disturbances.

Before solving this problem, there are two issues that deserve preliminary discussion: (i) how to generate the slip set point λ^*; and (ii) how to measure or estimate the slip λ in order to be used in feedback. Ideally, the slip set point should be selected such that the tyre–road friction is maximised, that is, $\lambda^* = \arg\max_\lambda \mu(\lambda)$, which is not easy due to the uncertainty in $\mu(\lambda)$. To overcome this hindrance, identification schemes to infer the friction peak before the slip control activation can be used (see, e.g. [25,27]) or a fixed λ^* can be employed as a compromise value for the most representative road surfaces found in practice. Further, the vehicle speed v is not easy to measure during braking manoeuvres, hampering the λ calculation and feedback. To address this problem, it is common to implement vehicle velocity observers, see, for example, [24,27–29], and in what follows it is assumed that a sufficiently reliable speed estimate is available to the controller.

In view of Equations (9), (16) and (18), the error dynamics are defined as

$$\dot{e} = -\frac{p_1}{v}(\boldsymbol{\theta}^{\mathrm{T}}\boldsymbol{\Phi}(\lambda) - T_{\mathrm{w}} + \Delta(t, \lambda, v, \omega)), \tag{19}$$

where $\Delta(.)$ is a uniformly bounded disturbance torque, comprising all the model uncertainties, namely

$$\Delta(t, \lambda, v, \omega) = \Delta_{\Psi 1}(t, \lambda) + \Delta_{\Psi 2}(t, \lambda) - \Delta_\omega(t, \omega) + (1 - \lambda)p_2 r \Delta_v(t, v), \tag{20a}$$

$$|\Delta(t, \lambda, v, \omega)| \leq \overline{\Delta_{\Psi_2}} + \overline{\Delta_\omega} + p_2 r(\overline{\Delta_v} + \overline{\Delta_{\Psi 1}}) \leq \bar{\Delta} \tag{20b}$$

for all $(t, \lambda, v, \omega) \in [0, \infty) \times \Lambda \times \mathcal{D}$. Compared with the torque applied to the wheel during an emergency braking, the value of $\Delta(.)$ is relatively small and tends to be neglected in the majority of the slip control designs reported in the literature [3,9,21,30–34]. However, if the control law incorporates adaptive mechanisms to deal with the parameter uncertainty in $\boldsymbol{\theta}$ (which is the case in this work), the presence of these small disturbances may introduce parameter drifts and other stability issues, as discussed in [35]. With the aim of mitigating such problems, the adaptive controller will be endowed with a robust modification (the dead zone), which, to be effective, requires the knowledge of a bound for the model disturbance and, as will be clear in the following, also plays an important role in the controller tuning. Another important issue in the SC design is related with the appearance of v in the denominator of Equation (19), which makes the slip error dynamics infinitely fast as $v \to 0$ [21]. In practice, the controller must be disabled before the vehicle reaches a complete stop, and, in what follows, we will assume that the domain of interest during the slip regulation is constrained to $(v, \omega) \in \mathcal{D}^c = [v_o, \infty) \times [0, \infty) \subset \mathcal{D}$, where v_o is a positive speed threshold at which the SC is deactivated.

Inspired by the IO linearisation technique previously discussed, the stabilisation of the error dynamics (19) will be achieved with the following control law:

$$T_{\mathrm{w}} = \hat{\boldsymbol{\theta}}^{\mathrm{T}}\boldsymbol{\Phi}(\lambda) - vke, \tag{21}$$

where k is a positive tuning parameter and $\hat{\boldsymbol{\theta}}$ the estimate of $\boldsymbol{\theta}$, which will be defined by an adaptive mechanism. The first term in the previous relation can be interpreted, to some extent, as a compensation factor that deals with the nonlinear tyre–road friction, while the second term represents a proportional term that improves the convergence. Substituting Equation (21) in Equation (19) yields

$$\dot{e} = -p_1 ke - \frac{p_1}{v}(-(\hat{\boldsymbol{\theta}} - \boldsymbol{\theta})^{\mathrm{T}}\boldsymbol{\Phi}(\lambda) + \Delta(.)). \tag{22}$$

To design the adaption law for $\hat{\boldsymbol{\theta}}$, consider the following candidate Lyapunov function:

$$V(e_\varepsilon, \tilde{\boldsymbol{\theta}}) = \frac{1}{2}e_\varepsilon^2 + \frac{p_1}{2\gamma}\tilde{\boldsymbol{\theta}}^{\mathrm{T}}\tilde{\boldsymbol{\theta}}, \tag{23}$$

where $\tilde{\boldsymbol{\theta}} = \hat{\boldsymbol{\theta}} - \boldsymbol{\theta}$ is the parametric estimation error, γ a constant tuning parameter and e_ε the regulation error with dead zone (ε) [36]

$$e_\varepsilon = g(e) = \begin{cases} 0 & \text{if } |e| < \varepsilon, \\ e - \varepsilon\ \mathrm{sgn}(e) & \text{if } |e| \geq \varepsilon, \end{cases}$$

and

$$\dot{e}_\varepsilon = g'(e)\dot{e} = \begin{cases} 0 & \text{if } e_\varepsilon = 0, \\ \dot{e} & \text{if } e_\varepsilon \neq 0. \end{cases} \tag{24}$$

In order to study the stability and transient behaviour of the system under closed loop, the time derivative of V

$$\dot{V} = e_\varepsilon \dot{e}_\varepsilon + \frac{p_1}{\gamma}\tilde{\boldsymbol{\theta}}^{\mathrm{T}}\dot{\tilde{\boldsymbol{\theta}}} \tag{25}$$

will be analysed in two parts. At first, we consider $e_\varepsilon \neq 0$, which enables us to replace $\dot{e}_\varepsilon$ with $\dot{e}$ (see Equation (24)), thus obtaining

$$\dot{V} = e_\varepsilon \dot{e} + \frac{p_1}{\gamma}\tilde{\boldsymbol{\theta}}^{\mathrm{T}}\dot{\tilde{\boldsymbol{\theta}}} \quad \forall e_\varepsilon \neq 0 \tag{26a}$$

$$= -\frac{p_1}{v}e_\varepsilon(-(\hat{\boldsymbol{\theta}} - \boldsymbol{\theta})^{\mathrm{T}}\boldsymbol{\Phi}(\lambda) + vke + \Delta(.)) + \frac{p_1}{\gamma}\tilde{\boldsymbol{\theta}}^{\mathrm{T}}\dot{\tilde{\boldsymbol{\theta}}}, \tag{26b}$$

$$\leq -p_1 k e_\varepsilon e + \frac{p_1}{v}\bar{\Delta}|e_\varepsilon| + p_1\tilde{\boldsymbol{\theta}}^{\mathrm{T}}\left(\frac{e_\varepsilon}{v}\boldsymbol{\Phi}(\lambda) + \frac{\dot{\tilde{\boldsymbol{\theta}}}}{\gamma}\right) \quad \forall e_\varepsilon \neq 0. \tag{26c}$$

To cancel out the last term in the previous relation, the adaption law is selected as

$$\hat{\boldsymbol{\theta}}(t) = \hat{\boldsymbol{\theta}}(t_i) - \int_{t_i}^{t} \gamma \frac{e_\varepsilon(\tau)}{v(\tau)}\boldsymbol{\Phi}(\lambda(\tau))\,\mathrm{d}\tau, \tag{27}$$

where $\hat{\boldsymbol{\theta}}(t_i)$ is the initial estimate of $\boldsymbol{\theta}$ and t_i the activation instant of the controller. It is worth pointing out that the adaption law described above is frozen when $e_\varepsilon = 0$, or equivalently $|e| \leq \varepsilon$, and the adaptation gain gets smaller as speed increases. Moreover, noticing that, for $e_\varepsilon \neq 0$, $e = e_\varepsilon + \varepsilon\ \mathrm{sgn}(e) = e_\varepsilon + \varepsilon\ \mathrm{sgn}(e_\varepsilon)$, one has

$$\dot{V} \leq -p_1 k e_\varepsilon^2 - p_1 k|e_\varepsilon|\left(\varepsilon - \frac{\bar{\Delta}}{vk}\right) \quad \forall e_\varepsilon \neq 0. \tag{28}$$

Since $(v, \omega) \in \mathcal{D}^c$, we can select the dead zone as $\varepsilon > \bar{\Delta}/(kv_0)$ to achieve $\dot{V} \leq -p_1 k e_\varepsilon^2$ for any $e_\varepsilon \neq 0$, which concludes the analysis of the first case. In the second case, $e_\varepsilon = 0$ and it is easy to check that $\dot{V}(0, \tilde{\boldsymbol{\theta}}) = 0$. Hence, joining the two cases, we get

$$\dot{V} \leq -p_1 k e_\varepsilon^2 \quad \forall e_\varepsilon. \tag{29}$$

The next proposition states the stability properties of the closed-loop system (Figure 5).

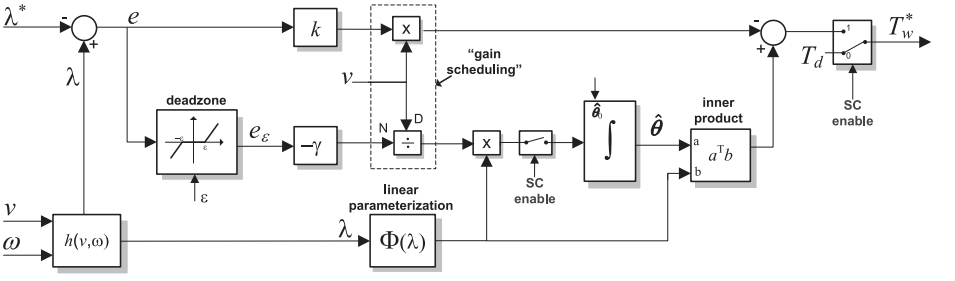

Figure 5. Block diagram of the proposed adaptive wheel slip control; the flag 'SC enabled' is generated by the braking supervisor in order to activate/deactivate the SC.

PROPOSITION 3.1 *Consider the control law* (21), (27) *applied to Equation* (19) *with* $k > 0$, $\gamma > 0$ *and* $\varepsilon > \bar{\Delta}/(kv_0)$. *It holds that*

(i) *the signals* e_ε *and* $\tilde{\boldsymbol{\theta}}$ *are bounded*;
(ii) *the signal* e_ε *is asymptotically vanishing, that is,* $\lim_{t\to\infty} |e_\varepsilon(t)| = 0$;
(iii) *the transient response performance can be quantified as follows*:

$$\|e_\varepsilon\|_{\mathcal{L}_2} \leq \sqrt{\frac{e_\varepsilon(0)^2}{2p_1k} + \frac{\|\tilde{\theta}(0)\|^2}{2k\gamma}}, \tag{30}$$

where $e_\varepsilon = g(e)$ *is the regulation error with dead zone defined in Equation* (24).

Proof The fact (i) can be deduced from the Lyapunov method: since Equation (23) is positive definite, and the time derivative $\dot{V}(e_\varepsilon, \tilde{\boldsymbol{\theta}}) \leq -p_1 k e_\varepsilon^2 \leq 0$ is negative semi-definite, then e_ε and $\tilde{\boldsymbol{\theta}}$ belong to $\mathcal{L}_\infty$, thus being bounded. Furthermore, integrating Equation (29), one has

$$e_\varepsilon^2 \leq -\frac{\dot{V}}{p_1k} \Rightarrow \lim_{t\to\infty} \int_0^t e_\varepsilon(\tau)^2 \,\mathrm{d}\tau \leq \frac{V(0) - \lim_{t\to\infty} V(t)}{p_1k} \leq \frac{V(0)}{p_1k}, \tag{31}$$

where the last inequality comes from the fact that V is lower bounded and $\dot{V} \leq 0$, which implies that $\lim_{t\to\infty} V(t)$ is finite [36]. It can also be straightforwardly verified that $\dot{V}$ is uniformly continuous ($\ddot{V} \leq -2p_1 k e_\varepsilon \dot{e}_\varepsilon$ is bounded), and by the application of Barbalat's lemma [36]: $\lim_{t\to\infty} \dot{V}(t) = 0$, which implies (ii). Finally, from Equation (31) an upper bound for the $\mathcal{L}_2$ norm of e_ε can be found as

$$\|e_\varepsilon\|_{\mathcal{L}_2} = \sqrt{\lim_{t\to\infty} \int_0^t e_\varepsilon(\tau)^2 \,\mathrm{d}\tau} \leq \sqrt{\frac{V(0)}{p_1k}} = \sqrt{\frac{(1/2)e_\varepsilon(0)^2 + (p_1/2\gamma)\|\tilde{\boldsymbol{\theta}}(0)\|^2}{p_1k}}, \tag{32}$$

thus proving (iii). ■

Remark 3.1 The results presented in the previous proposition characterise the controller performance and allow us to understand how the controller parameters (ε, k, γ) affect the slip error response. For instance, e_ε being vanishing implies that the steady-state regulation error e will converge asymptotically to the set $\{|e| \leq \varepsilon\}$. Therefore, the selection of the dead zone ε, besides the robustness considerations mentioned above, can also take into account the wheel slip measurement noise, for example, letting $\varepsilon \geq \max(\sigma_\lambda, \bar{\Delta}/(kv_0))$, where σ_λ is the precision associated with the λ measure (or estimation). In terms of transient performance, Equation (30) suggests that the designer can reduce the $\mathcal{L}_2$ norm of the regulation error by decreasing the initial estimation error ($\|\tilde{\boldsymbol{\theta}}(0)\|$) and initial regulation error ($e_\varepsilon(0)$), or by increasing the gains k, γ.

Remark 3.2 The SC will be switched on by the braking supervisor when excessive tyre slip is detected. Assuming that this activation occurs at $t = t_i$, we have $T_w(t) = T_d(t)$ for $t < t_i$, while for $t \geq t_i$, the wheel torque will be provided by Equation (21). At the activation instant, the torque generated by the controller will be defined as $T_w(t_i) = \hat{\boldsymbol{\theta}}(t_i)^T \boldsymbol{\Phi}(\lambda(t_i)) - kv(t_i)e(t_i)$ and, as a result, if the controller is not carefully initialised, discontinuities in the wheel torque signal may occur (i.e. $T_d(t_i) \neq T_w(t_i)$). To avoid this undesirable behaviour, the initial estimative of $\boldsymbol{\theta}$ is rescaled as follows:

$$\hat{\boldsymbol{\theta}}(t_i) = \boldsymbol{\theta}_N \frac{T_d(t_i) + kv(t_i)e(t_i)}{\boldsymbol{\theta}_N^T \boldsymbol{\Phi}(\lambda(t_i))}, \tag{33}$$

where $\boldsymbol{\theta}_N$ is an initial parameter estimate chosen by the designer.

Remark 3.3 The vehicle speed plays a very important role in the SC response and robustness disturbances capabilities. For example, by analysing the control law (21), it is clear that there is an equivalent proportional error term (vke) that is directly proportional to the vehicle speed, while an opposite influence is observed in the adaptation mechanism (27), that is, the adaptation rate gets smaller at higher speed. In a way, this can be interpreted as a gain-scheduled mechanism, which was already discussed in previous works on wheel slip control within linear (or linearisation) frameworks [3,21,30], and is extended in this article for the robust adaptive controller. Another aspect that is worth mentioning is the influence of v on the SC robustness. To explain this, consider the time derivative of the Lyapunov (28): the term associated with the disturbance (upper bound) $\bar{\Delta}$ decreases at higher speeds, and the minimum value for the dead zone ε also gets smaller. Consequently, these results suggest that the SC may deal more easily with the disturbances at higher vehicle speeds. From a practical point of view, these observations are in accordance with the fact that the speed estimation is affected by large errors as the vehicle velocity decreases, for example, due to delays introduced by the wheel encoders signal-processing phases [9].

Remark 3.4 It is also interesting to analyse the influence of the vehicle velocity v into the tyre slip dynamics (9) (or equivalently in the error dynamics (19) from a different perspective, that is, by looking at v as a slowly time-varying parameter. For example, in the ideal scenario of no uncertainty in the model (i.e. Ψ is known and $\Delta_v = \Delta_w = 0$), it was shown in Section 3.1 that the IO linearisation technique renders a closed-loop slip response independent of the vehicle speed and with exponential convergence to λ^* (see Equation (10)). In this case, we can treat the vehicle velocity dynamics (5a) as the 'zero dynamics' of the system [22], which is input-to-state stable during the slip control operation. On the other hand, when we take into account the model uncertainties and employ the adaptive controller, the IO linearisation is no longer 'perfect' and the vehicle speed appears in the slip closed-loop dynamics (see Equation (22), which is then incorporated into the adaptive law and, as discussed in the previous remark, attenuates the disturbance effects. Consequently, in this latter case, we can look again at the v dynamics as the 'zero dynamics' of the system or, in alternative, neglect these dynamics and assume that v is a slow time-varying parameter. The latter approach, considered also in [3,9,21], is justified owing to the large difference of equivalent inertias between the wheel and the vehicle chassis.

4. Wheel braking torque allocator

The wheel SC proposed in the previous section only specifies the desired wheel torque (T_w), but does not define how this torque should be split between the friction brakes (T_f) and the

electric motor (T_e). This assignment is performed in a second step, after discretising the SC, using a torque distribution strategy based on the CA concept, see for example, [11,12,37]. As primary objective, the CA must ensure that the requested torque, T_w, is produced by the braking devices, that is,

$$T_w = T_f + T_e \tag{34}$$

complying, at the same time, with the range and variation rate limits, defined in (4). Given that the system is discretised with a sampling time t_s, the derivative $\dot{T}_i$ can be approximated by the forward Euler method as $\dot{T}_i \simeq (T_i[k] - T_i[k-1])/t_s$, and the range and rate constraints can be joined together as

$$\underline{T_i} \leq T_i \leq, \overline{T_i}, \quad i \in \{e,f\}, \tag{35a}$$

$$\underline{T_i} = \max(T_{i,\min}, T_i[k-1] - t_s\dot{T}_{i,\max}), \tag{35b}$$

$$\overline{T_i} = \min(T_{i,\max}, T_i[k-1] + t_s\dot{T}_{i,\max}). \tag{35c}$$

Thus, the number of inequalities constraints is reduced from four to only two per actuator. Notice that, for a given torque request T_w, there may be several pairs (T_f, T_e) that satisfy Equation (34). Accordingly, this redundancy can be exploited by the CA to select the pair (T_f, T_e) that maximises the energy efficiency and optimises the (wheel) torque dynamic response. For instance, it is well known that the regenerative braking capabilities of IWMs are much more energy efficient than the friction brakes, hence the use of the latter braking device should be, whenever possible, penalised. Furthermore, the IWMs torque response offers a much larger bandwidth than the friction brakes (Figure 6), albeit with less control authority, and the torque allocation should also take into account the frequency content of the T_w signal, for example, making T_e more sensitive to the high-frequency content in T_w. Taking into consideration these ideas together with the constraints (34) and (35), the wheel torque allocation can be formulated as the following optimisation problem:

$$\begin{aligned} \min_{T_f,T_e} \quad & (\alpha_f T_f^2 + \alpha_e(T_e)T_e^2) + (\beta_f(T_f - T_f[k-1])^2 + \beta_e(T_e - T_e[k-1])^2) \\ \text{s.t.} \quad & T_f + T_e = T_w, \quad \underline{T_i} \leq T_i \leq, \overline{T_i}, \quad i \in \{e,f\}. \end{aligned} \tag{36}$$

The cost function of the previous problem can be divided into two components. The first term assigns a penalty to the use of each braking actuator, using for this purpose the weights α_f and $\alpha_e(.)$, which are associated with the frictional braking and IWM, respectively. As the IWM has two operational modes, that is, regeneration and acceleration, it is also helpful to assign

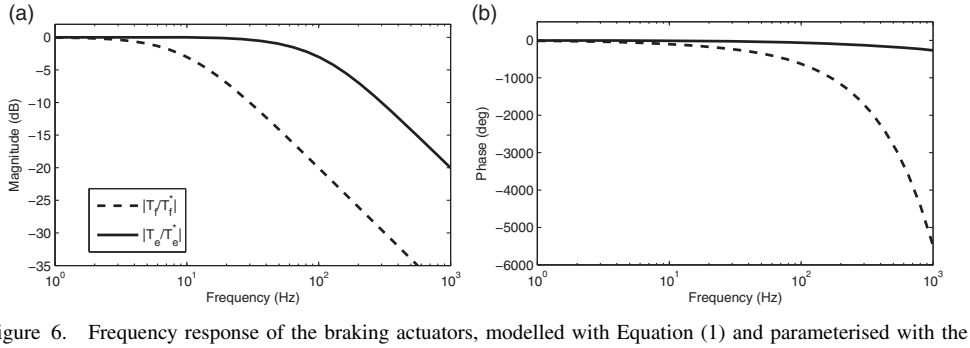

Figure 6. Frequency response of the braking actuators, modelled with Equation (1) and parameterised with the values given in Appendix 1.

different penalisation values to each of these modes. To address this issue, we make the weight $\alpha_e(.)$ dependent on the T_e signal as

$$\alpha_e(T_e) = \begin{cases} \alpha_e^- & T_e < 0, \\ \alpha_e^+ & T_e \geq 0, \end{cases} \tag{37}$$

where the parameters α_e^+, α_e^- are related with the regeneration and acceleration mode, respectively. Despite being unusual, the IWM acceleration mode can also be employed during braking manoeuvres, and, in Section 6, some examples will be shown where this property is very useful to quickly reduce the wheel moment during the slip transients. Moreover, to exploit the different bandwidths of the braking devices, the second term in the cost function (36) assigns, via the weights β_i, penalties to torque variations in each actuator.

Albeit the complexity of Equation (36) is not very high, the inclusion of nonlinearities, coupled with the inequality constraints, makes it difficult to find a closed-form solution. In order to gain some insight in the above problem, we start by considering a simplified case with $\alpha(T_e)$ constant and with no inequalities constraints, which yields an optimisation linear problem. Then, the above assumptions will be removed and a numerical solver derived to handle the general case.

4.1. *Linear filtering approximation*

For the cases where none of the braking devices is saturated (including range and rate limits) and the electric torque limits satisfy

$$sgn(\underline{T_e}) = sgn(\overline{T_e}), \tag{38}$$

the solution of the allocation problem is a simple linear filter, as outlined in the next proposition.

PROPOSITION 4.1 *Assume that Equation* (38) *holds, which implies that* $\alpha_e(.) = \alpha_e$ *is constant, and that the inequality constraints in the CA problem* (*36*) *are inactive. Under these assumptions, the optimal solution of the control allocator is given by the following discrete-time filters*

$$\frac{T_f}{T_w}(z) = \frac{\alpha_e + \beta_e}{l}\frac{z - a_f}{z - p}, \quad \frac{T_e}{T_w}(z) = \frac{\alpha_f + \beta_f}{l}\frac{z - a_e}{z - p}, \tag{39a}$$

$$a_f = \frac{\beta_e}{\alpha_e + \beta_e}, \quad a_e = \frac{\beta_f}{\alpha_f + \beta_f}, \quad p = \frac{\beta_f + \beta_e}{l}, \tag{39b}$$

$$l = \alpha_f + \alpha_e + \beta_f + \beta_e, \tag{39c}$$

where z represents the Z-transform operator.

Proof Ignoring the inequality constraints in Equation (36), the Lagrangian function of the resulting optimisation problem is given by

$$\begin{aligned} \mathcal{L}(T_f, T_e, \lambda_L) = {} & \alpha_f T_f^2 + \alpha_e T_e^2 + \beta_f (T_f - T_f[k-1])^2 + \beta_e (T_e - T_e[k-1])^2 \\ & + \lambda_L (T_f + T_e - T_w), \end{aligned} \tag{40}$$

where λ_L is the Lagrange multiplier. Applying the first-order optimality conditions [38], we get

$$\frac{\partial \mathcal{L}}{\partial T_f} = 2\alpha_f T_f + 2\beta_f (T_f - T_f[k-1]) + \lambda_L = 0, \tag{41a}$$

$$\frac{\partial \mathcal{L}}{\partial T_e} = 2\alpha_e T_e + 2\beta_e (T_e - T_e[k-1]) + \lambda_L = 0, \tag{41b}$$

$$\frac{\partial \mathcal{L}}{\partial \lambda_L} = T_f + T_e - T_w = 0. \tag{41c}$$

Solving the previous equations, the optimal solution has the form

$$\begin{bmatrix} T_f \\ T_e \end{bmatrix} = \underbrace{\frac{1}{l}\begin{bmatrix} \beta_f & -\beta_e \\ -\beta_f & \beta_e \end{bmatrix}}_{\boldsymbol{A}} \begin{bmatrix} T_f[k-1] \\ T_e[k-1] \end{bmatrix} + \underbrace{\frac{1}{l}\begin{bmatrix} \alpha_e + \beta_e \\ \alpha_f + \beta_f \end{bmatrix}}_{\boldsymbol{B}} T_w. \tag{42}$$

Defining the shift operator q, $q^{-1}T[k] = T[k-1]$, Equation (42) can be written as

$$\begin{bmatrix} T_f[k] \\ T_e[k] \end{bmatrix} = \boldsymbol{A}\begin{bmatrix} T_f[k-1] \\ T_e[k-1] \end{bmatrix} + \boldsymbol{B}T_w[k] = q^{-1}\boldsymbol{A}\begin{bmatrix} T_f[k] \\ T_e[k] \end{bmatrix} + \boldsymbol{B}T_w[k], \tag{43}$$

which is equivalent to

$$\begin{bmatrix} T_f[k] \\ T_e[k] \end{bmatrix} = (q\boldsymbol{I} - \boldsymbol{A})^{-1} q\boldsymbol{B}T_w[k], \tag{44}$$

where $\boldsymbol{I}$ is the identity matrix. Therefore, computing $(q\boldsymbol{I} - \boldsymbol{A})^{-1}q\boldsymbol{B}$, the filters given in Equation (39) are obtained. ■

Remark 4.2 The stability of Equation (39) is ensured provided that the magnitude of p is less than 1 (e.g. by selecting $\alpha_i \neq 0$). Further, if the filter zero cancels the pole (e.g. by selecting $\beta_f = \beta_e = 0$ or $\alpha_f = \alpha_e = 0$), the filter reduces to a constant gain.

Additional understanding of the CA solution can be gained by inspecting the frequency response of the linear filters (39), depicted in Figure 7. The first plot (Figure 7(a)), illustrates the allocation among (T_f, T_e) when $\beta_f = \beta_e = 0$, and highlights that a 'static', that is, equal for all frequencies, is obtained. Actually, the steady-state gain of the filters (39) is given by

$$\frac{T_f}{T_w}(z=1) = \frac{\alpha_e}{\alpha_f + \alpha_e}, \quad \frac{T_e}{T_w}(z=1) = \frac{\alpha_f}{\alpha_f + \alpha_e}. \tag{45}$$

Thus, it is not surprising to verify that the β_i parameter has no influence on the DC gain. On the other hand, when non-zero β_i values are used, the allocation will be sensitive to the frequency spectrum of the input torque T_w; in the example illustrated in Figure 7(b), T_e and T_f respond to the high- and low-frequency contents, respectively. Therefore, the CA parameters can also be tuned from a frequency response perspective, and, in a later section, we will show that by a proper selection of α_i, β_i, the frequency response of (T_f, T_e) can be, somehow, shaped. As a side note, the frequency response plots also show that the magnitude of the combined torque response $(T_f + T_e)/T_w$ is always unitary, which is in accordance with the expectations associated with the equality constraint (34).

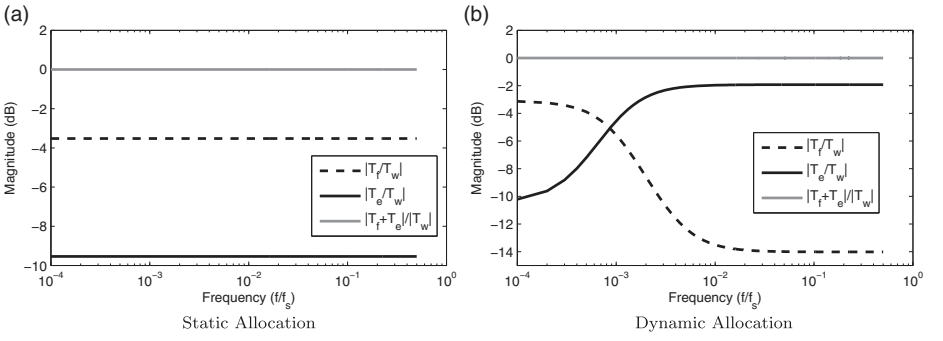

Figure 7. Frequency response of the wheel torque allocation: (a) static allocation, generated from the state 3 in Table 1 and (b) dynamic allocation, generated from the state 4 in Table 1; The frequency scale is normalised with the sampling frequency ($f_s = 1/t_s$) and it is assumed that $\overline{T_e} > \underline{T_e} > 0$.

4.2. *Numerical solver for $\alpha_e(.)$ constant*

In this section, we will continue to work under the assumption that Equation (38) holds, but a numerical solver is introduced to handle the inequality constraints. Given that the CA will be deployed in real-time control system, with limited computing resources, numerically efficient solvers, such as the active set methods [39], represent one of the possible candidates to calculate the solution of Equation (36). Nonetheless, in view of the reduced number of inequalities (four), a simple solution can be found by following the next three steps:

(1) check if the requested torque T_w is feasible:

$$\boldsymbol{T} = (T_f, T_e) = \begin{cases} (\overline{T_f}, \overline{T_e}) & \text{if } T_w > \overline{T_f} + \overline{T_e}, \\ (\underline{T_f}, \underline{T_e}) & \text{if } T_w < \underline{T_f} + \underline{T_e}, \\ \text{go to step 2} & \text{otherwise} \end{cases} \tag{46}$$

(this step will ensure that, if T_w is unfeasible, the difference between the allocated torque and T_w is minimised, see Figure 8(c)).

(2) compute the unconstrained optimal solution $\boldsymbol{T}^u = (T_f^u, T_e^u)$ by applying the difference equations resulting from Equation (39); if this solution fulfils the inequality constraints, then $\boldsymbol{T} = \boldsymbol{T}^u$ and the solution is found (Figure 8(a)), otherwise go to step 3.

(3) In this case, the requested torque T_w is feasible, but $\boldsymbol{T}^u$ does not fulfil the inequality constraints and, as a consequence, at least one inequality is active. Notice, however, that the activation of one inequality, together with the equality constraint in Equation (36), defines a unique solution. Activating individually each one of the problem inequalities results in the following candidate solutions: $\{(T_w - \overline{T_e}, \overline{T_e}), (T_w - \underline{T_e}, \underline{T_e}), (\overline{T_f}, T_w - \overline{T_f}), (\underline{T_f}, T_w - \underline{T_f})\}$; among these, we neglect the ones that violate the problem inequalities and the optimal solution is the one that minimises the cost function (Figure 8(b)).

4.3. *Numerical solver for the general case*

This section addresses the general problem (36), dropping the assumption of constant $\alpha_e(T_e)$ suggested by condition (38). In order to deal with this situation, our approach consists in dividing the original allocation problem into two sub-problems. In the first, we compute a solution assuming that the IWM can only produce regenerative braking, while in the second, the opposite case will be considered, that is, the IWM is only allowed to generate the acceleration

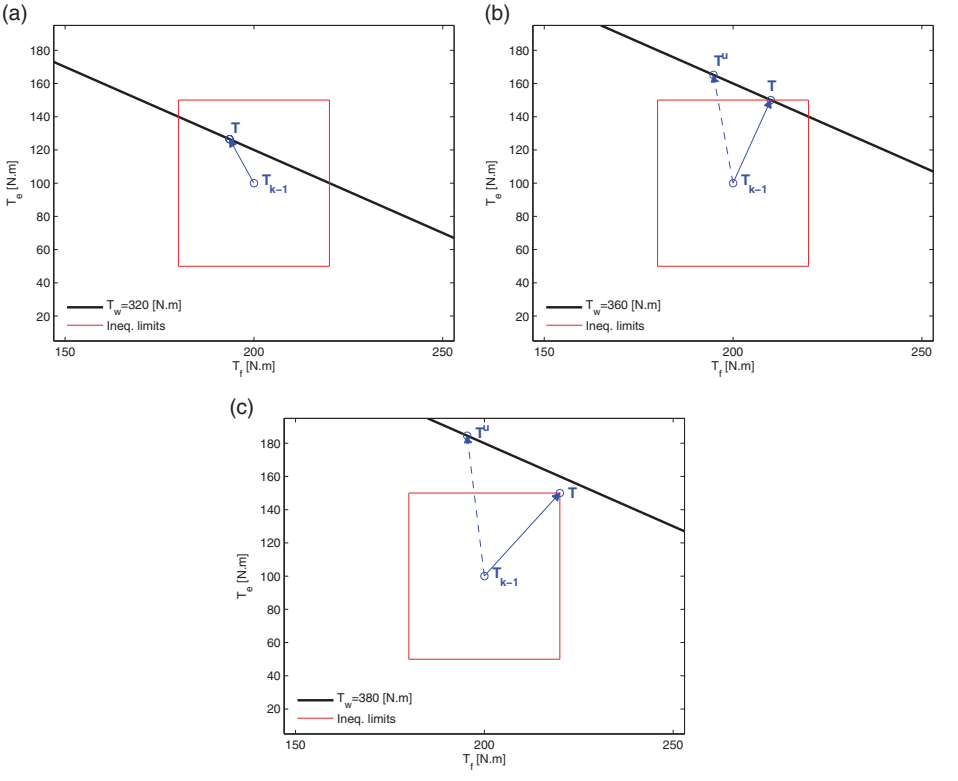

Figure 8. Example of operation for the wheel torque allocator: (a) unconstrained solution does not violate the constraints, (b) unconstrained solution is outside the acceptable domain and, as a result, it is necessary to activate one constraint and (c) T_w is unfeasible.

torque. Notice that in each of these sub-problems, condition (38) is always verified, thus we can employ the solver described in the previous section. Based on these arguments, the final numerical solver is described as follows:

(1) Check the feasibility of the problem, as in Equation (46). If it is feasible go to the next step, otherwise extract the closest point to T_w.
(2) At this point, we know that there is, at least, one feasible solution. The basic idea now, is to calculate two types of solutions:
   (i) determine $\boldsymbol{T}^+$, that is, the best allocation with regenerative braking, using the solver in the previous section, configured with $\alpha_2 = \alpha_2^+$ and $T_{e,min} = 0$;
   (ii) determine $\boldsymbol{T}^-$, that is, the best allocation by accelerating the electric motor, employing the solver described in the previous section, configured with $\alpha_2 = \alpha_2^-$ and $T_{e,max} = 0$;
   (iii) from the candidates $\{\boldsymbol{T}^+, \boldsymbol{T}^-\}$, discard the ones that violate the equality or inequalities constraints; for the resulting candidates, evaluate the cost function in Equation (36): the optimal is the one with minimum cost.

Therefore, the above algorithm is numerically simple, has a well-defined number of maximum iterations and it is suitable for realtime implementation.

4.4. *Procedure to select the allocator weights*

One natural issue that emerges in the torque allocator implementation is the selection procedure of the weights α_i and β_i, which must take into account the actuators characteristics, designers preferences and the EV operational mode. To help the designer in this process, let us define the torque-sharing ratio between the IWM and the friction brakes, as

$$\rho = \left| \frac{T_\mathrm{e}}{T_\mathrm{f}} \right|. \tag{47}$$

Considering the linear filters (39), this variable can also be made frequency dependent, that is,

$$\begin{aligned} \rho(f) &= \left| \frac{T_\mathrm{e}}{T_\mathrm{f}}(z = \mathrm{e}^{j2\pi f t_\mathrm{s}}) \right| \\ &= \left| \left(\frac{\alpha_\mathrm{f} + \beta_\mathrm{f}}{\alpha_\mathrm{e} + \beta_\mathrm{e}} \right) \frac{\mathrm{e}^{j2\pi f t_\mathrm{s}} - \beta_\mathrm{f}/(\alpha_\mathrm{f} + \beta_\mathrm{f})}{\mathrm{e}^{j2\pi f t_\mathrm{s}} - \beta_\mathrm{e}/(\alpha_\mathrm{e} + \beta_\mathrm{e})} \right| \\ &= \left(\frac{\alpha_\mathrm{f} + \beta_\mathrm{f}}{\alpha_\mathrm{e} + \beta_\mathrm{e}} \right) \frac{\sqrt{1 + (\beta_\mathrm{f}/(\alpha_\mathrm{f} + \beta_\mathrm{f}))^2 - 2(\beta_\mathrm{f}/(\alpha_\mathrm{f} + \beta_\mathrm{f}))\cos(2\pi f t_\mathrm{s})}}{\sqrt{1 + (\beta_\mathrm{e}/(\alpha_\mathrm{e} + \beta_\mathrm{e}))^2 - 2(\beta_\mathrm{e}/(\alpha_\mathrm{e} + \beta_\mathrm{e}))\cos(2\pi f t_\mathrm{s})}}. \end{aligned} \tag{48}$$

Now, assume that the designer specifies some desired torque-sharing values (ρ_j^*) for a series of frequencies (f_j):

$$\mathcal{S} = \{(f_1, \rho_1^*), (f_2, \rho_2^*), \ldots, (f_N, \rho_N^*)\}. \tag{49}$$

As an example, Figure 9(a) shows a possible shape for ρ^*, which provides the designer a simple framework to specify the low-/high-frequency gains, as well as a transition zone (middle frequencies). The question now is how we can select the parameters α_i, β_i in order to generate a torque-sharing ratio ρ close to the desired ρ^*; given the mathematical expression for the frequency response (48), this selection is far from being trivial. To overcome this issue, we propose to solve the following nonlinear least squares problem:

$$\min_{\alpha_\mathrm{f}, \alpha_\mathrm{e}, \beta_\mathrm{f}, \beta_\mathrm{e}} \sum_{j=1}^{N} (\rho_j^* - \rho(f_j))^2 \tag{50}$$

which, using a numerical solver, enables us to find a suitable set of torque allocator weights. Figure 9(b) illustrates an application example of this methodology for the case of parallel braking (i.e. using both friction brakes and IWM).

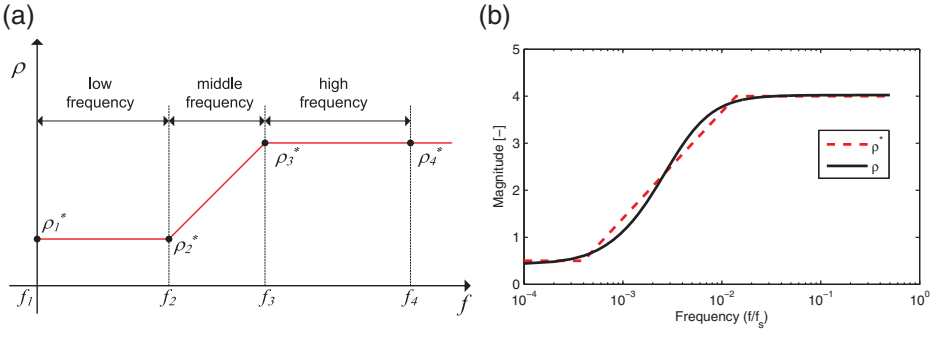

Figure 9. (a) Shape of the desired torque-sharing ratio ρ^* employed in this article and (b) reference ρ^* employed to design the state 4 of the torque supervisor (Table 1) and the approximating ρ (obtained after solving Equation (50)).

Table 1. Example of operating modes for the braking supervisor.

Number	State	α_f	α_e^+	α_e^-	β_f	β_e	SoC	SC enable
1	Series braking	0.2	0	0.8	0	0	$< \text{SoC}_{th}$	0
2	Series ABS	0	0	0.024	0.8	0.2	$< \text{SoC}_{th}$	1
3	Parallel braking	0.2	0.4	0.8	0	0	$\geq \text{SoC}_{th}$	0
4	Parallel ABS	0.002	0.005	0.01	0.8	0.2	$\geq \text{SoC}_{th}$	1
5	IWM failure	0	1	1	0	0	–	0/1

5. Braking supervisor

In order to take full advantage of wheel torque allocator, the parameters α_i and β_i should be modified depending on the EV running conditions. This adaptation is performed by the braking supervising unit (Figure 3), which is also responsible for the activation/deactivation of the wheel SC. As an illustrative example, Table 1 shows the braking operation modes considered in this work, which are divided into series/parallel braking with the SC enabled/disabled. The series terminology refers to the fact that, during normal braking, the friction brakes are only employed when the electrical torque saturates, while the parallel braking uses always both braking devices. The first mode, series braking, is available when the SoC of the energy source is not high (i.e. below a threshold SoC_{th}), and seeks to maximise the use of the regenerative braking; for that reason, the penalisation of the friction brakes is higher than that for regenerative braking ($\alpha_f \gg \alpha_e^+$). On the other hand, when the SoC is close to the full charge, it may be convenient to reduce, gradually, the amount of regenerative braking and start to apply parallel braking (assigning higher penalisation to the electric motor usage, α_e^+), which is addressed by the operational modes 3 and 4. A final state (number 5) is also added to contemplate the situation where the IWM fails and only the friction brakes are available.

It is worth mentioning that, in both series and parallel braking, when an emergency situation is detected and the SC enabled, the energy efficiency metric is no longer the main factor in the torque blending; in these scenarios, safety and a good slip regulation supersede the energy metric as the top priority. For those reasons, when the braking supervisor switches to the states 2 and 4, the weights associated with the dynamic allocation (β_i) assume preponderance in the torque allocation, and are tuned with the aim of exploiting the different actuation bandwidth offered by the braking devices (e.g. employing the procedure described in Section 4.4). A special mention is also due to the weight α_e^-. This parameter is responsible for the penalisation assigned to the IWM acceleration mode and, except for the fault state, presents always a higher value than α_f and α_e^+, the penalties of friction and IWM braking. Even tough one may not expect to accelerate the IWM during normal braking manoeuvres, we will show in Section 6 that the SC can benefit from this feature. Furthermore, due to space constraints, the full details on the activation/deactivation logic of the SC, and also the switching conditions between states, are omitted here, but is sufficient to say that this logic uses the information $(\lambda, T_d, v, \text{SoC})$ to identify an emergency braking and perform the transitions.

To conclude, the proposed hybrid ABS structure is able to easily address the various scenarios that may affect the EV braking system (e.g. normal braking, emergency braking, low SoC, high SoC, full SoC, IWM fault, actuator constraints, etc.) and offers a simple tool to accommodate different braking approaches (series or parallel).

6. Simulation results

The performance of the proposed control strategy was evaluated in a co-simulation between CarSim [40] and Matlab/Simulink. The former tool is responsible for the vehicle dynamics

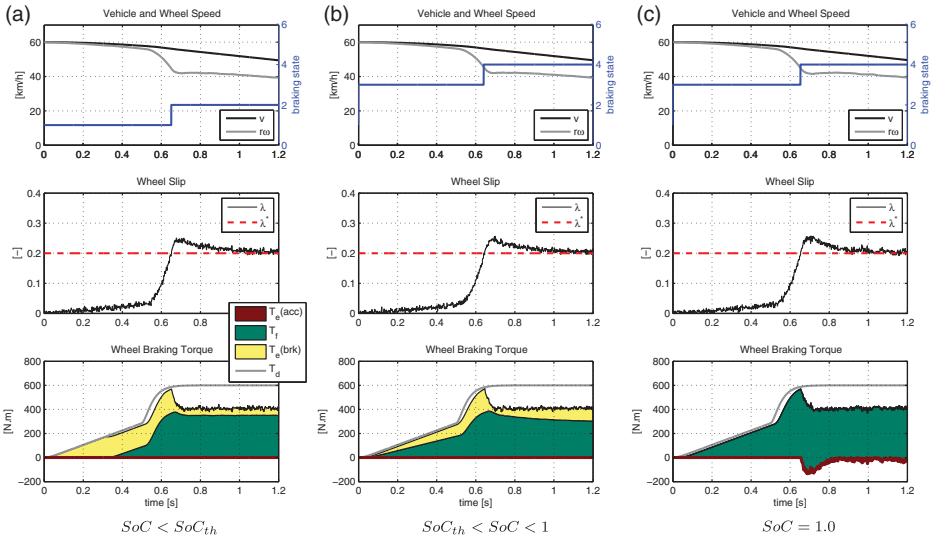

Figure 10. Simulation results for braking on wet asphalt ($\mu_{\max} = 0.6$) for different values of SoC ((a) SoC $<$ SoC_{th}, (b) SoC_{th} $<$ SoC $<$ 1 and (c) SoC $= 1.0$). The graphical representation of the wheel braking torque (T_{w}), and its allocation between electric and friction parts, is plotted in a stacked structure, where T_{w} is the result of summing $T_{\text{e}}(\text{acc}) + T_{\text{f}} + T_{\text{e}}(\text{brk})$; for convenience of discussion and illustration, the electric torque was split into regenerative ($T_{\text{e}}(\text{brk})$) and an acceleration ($T_{\text{e}}(\text{acc})$) components.

modelling and, compared with the QCM used in SC design, offers a more realistic environment to validate the braking control system. To complement CarSim, Matlab/Simulink is employed to implement the wheel SC, torque allocator, braking supervisor and the braking devices dynamics, parameterised with the values described in Appendix 1. A typical 'A-class' hatchback vehicle, available in the CarSim library, was used as the test car for the simulations, fitted with 175/70 R13 tyres and modelled with the magic tyre formula 5.2 [41]. Based on this simulation setting, several braking manoeuvres were carried out in a straight road, and, for simplicity, only the results of the left front wheel are shown (the other wheels have similar behaviour). To account for measurement errors, the slip λ was corrupted by a Gaussian noise with variance 0.005^2.

The first batch of tests, illustrated in Figure 10, aims at evaluating the hybrid ABS performance for three levels of battery SoC: low, high and full. Analysing the low SoC case (Figure 10(a)), two phases can be identified. In the first section, for $t \in [0, 0.65]$ s, a normal braking manoeuvre is performed: in order to maximise the energy efficiency, the torque allocator privileges the electric motor utilisation; the friction brakes only start to be applied after the electric torque reaches saturation, that is, a series braking approach is being applied. In the second part ($t > 0.65$ s), the tyre slip reaches high values and the SC is activated (note that the braking supervisor switches to the state 2): in this case, the torque allocation strategy uses the electric actuator to quickly decrease the wheel moment and keep the tyre slip near the set point, while the slow friction brakes torque is kept constant throughout the remaining of the manoeuvre. In the high SoC situation (Figure 10(b)), similar results to the low SoC case can be found, but with an important difference: since the beginning of the manoeuvre, a parallel braking policy is employed, enabling both electric and friction devices.

Finally, when the SoC reaches the full charge, the IWM is no longer able to provide regenerative braking, but this does not necessarily mean that the IWM should be disabled during the slip control phase. In fact, it turned out (Figure 10(c)) that we can still employ the IWM to produce, during some tenths of a second, the acceleration torque and, as a consequence, quickly

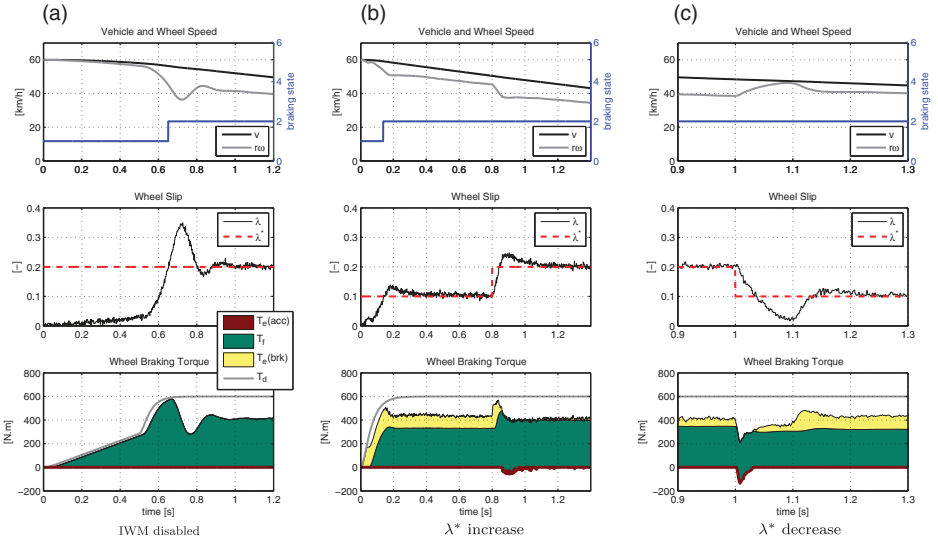

Figure 11. Simulation results for braking on wet asphalt ($\mu_{\max} = 0.6$) for different set points and the special case with IWM disabled; the wheel torque is plotted using a stacked representation, discussed in Figure 10: (a) IWM disabled, (b) λ^* increase and (c) λ^* decrease.

decrease the wheel moment required by the slip control after its activation; simultaneously, the friction torque is smoothly brought to its new steady-state value. Although this mode of operation, that is, accelerating the IWM during a braking manoeuvre, may look counterintuitive, the simulation results highlights that, even if no energy recuperation is possible, the IWM usage is still pivotal to provide a fast slip response and ensure a braking behaviour independent of the battery SoC. To emphasise this last point, and also for comparison purposes, Figure 11(a) shows the braking performance when the IWM is, for some reason, disabled (for example, motivated by a fault before the braking). Examining these results, it is visible that employing only T_f is sufficient to perform the slip regulation, but, due to the large time constant and delays in the friction brake actuator dynamics, some degradation is introduced in the transient response (larger overshoot and oscillations).

There are also others scenarios, like the appearance of strong disturbances during the slip regulation process, where the IWM assistance is beneficial. Some of these situations are illustrated in Figure 11(b) and (c) for set-point changes, and in Figure 12(b) for a μ jump; in all these cases, it can be observed that the wheel slip regulator is able to cope with the disturbances and the IWM torque (acceleration and braking) is, again, exploited to quickly bring the slip to the set point λ^*. As a matter of fact, analysing more closely the test with a λ^* decrease (Figure 11(c)), it is interesting to note that the friction brake torque is kept constant at ~ 300 N m, while the IWM torque is being modulated to respond to the disturbance, or, in other words, to provide the high-frequency content of the T_w signal. From a braking intensity point of view, there are also some cases, such as decelerations on low μ roads, where the regenerative torque is enough to provide all the vehicle braking needs, as illustrated in Figure 12(a).

Along with the torque allocation features, the adaptive mechanism incorporated into the slip control is also a key aspect in handling the model parametric uncertainties. To explain how this adaption works, Figure 13 shows the evolution of $\hat{\boldsymbol{\theta}}$ during the snow and μ jump tests. First, while a normal braking is detected, the output of the estimator is the same as the nominal estimate, $\boldsymbol{\theta}_N$, and the adaption is frozen. Next, once the slip control is activated the estimate is re-initialised with Equation (33) in order to avoid wheel torque jumps, as explained

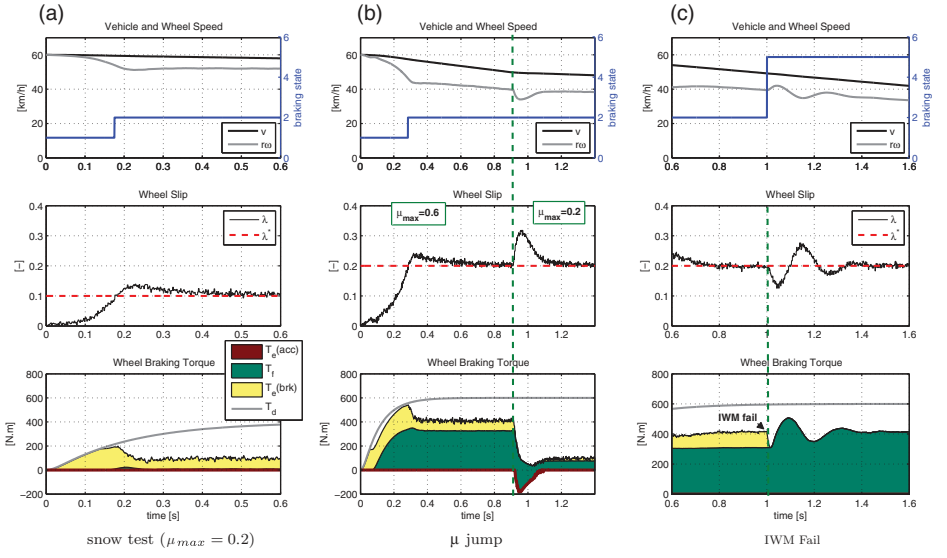

Figure 12. Simulation results for braking on low μ and response to μ jumps (SoC $<$ SoC_{th}); the wheel torque is plotted using a stacked representation, discussed in Figure 10: (a) snow test ($\mu_{\max} = 0.2$), (b) μ jump and (c) IWM fail.

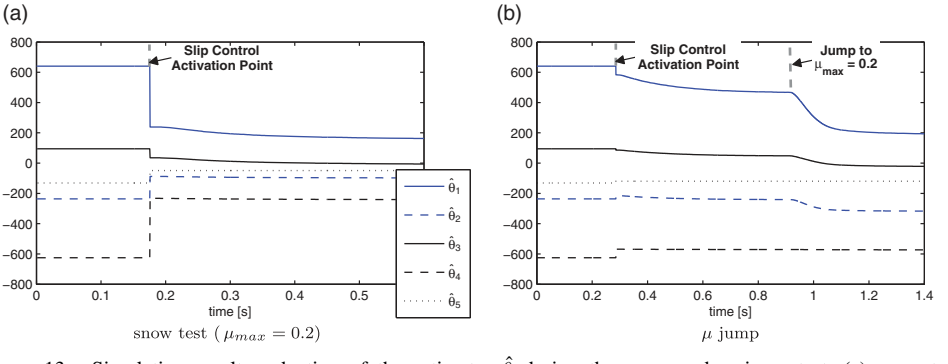

Figure 13. Simulation results: adaption of the estimates $\hat{\theta}$ during the snow and μ jump test: (a) snow test ($\mu_{\max} = 0.2$) and (b) μ jump.

in Section 3.3; after this step, the adaption begins and it can be observed a quick convergence to a steady-state value in the snow test, while in the μ jump case, there is further activity to track the friction change that occurs at approximately $t = 0.9$ s. Hence, these results indicate that, apart from the issue associated with the selection of the optimal λ^*, the proposed SC is robust to uncertainties in μ.

In a brake-by-wire system, one of the most important issues is how to handle failures in the braking devices. As a preliminary test, consider the case depicted in Figure 12(c), where the IWM fails around 1 s, forcing a rapid decrease of the electrical torque to zero. In that situation, the braking supervisor switches to a (IWM) fault mode (number 5), and reconfigures the torque allocator to employ only the remaining healthy actuator, the friction device. By inspecting the response after this fault injection, it can be seen that the friction actuator takes over the wheel torque and is, naturally, capable of recovering the slip control with minimum impact on the braking effectiveness. To a certain extent, the proposed braking structure is tolerant to some types of IWM failures, while more challenging failures scenarios (e.g. friction braking faults) will be tackled in future works.

7. Conclusion

In this work, a hybrid ABS solution for EVs and hybrid vehicles was proposed, endowed with IWMs and friction brakes. The proposed method relies on a robust adaptive wheel SC, and a wheel torque allocator to distribute the braking effort among the two actuators. Besides handling the actuators constraints, the torque allocator exploits the braking redundancy to optimise the energy efficiency and dynamic performance metrics. Simulation studies, carried out with the CarSim environment, highlighted that the IWM can assist the friction brakes, not only during normal braking manoeuvres, but also in emergency braking, contributing to a better transient response of the wheel SC. As future work, we plan to experimentally validate the hybrid ABS controller in a multi-motor EV prototype and investigate fault-tolerant schemes.

Acknowledgements

This work was partially funded by FCT – Science and Technology Foundation, through the scholarship number SFRH/BD/47882/2008. Thanks are also due to Alexandre Silveira and Pedro Melo for their valuable comments, which have helped to improve the readability of the article. Finally, we also appreciate the valuable discussion with Dr Jochen Rauh, during the IAVSD11 congress, which have helped to extend the functionalities of the torque allocator.

References

[1] C.C. Chan, A. Bouscayrol, and K. Chen, *Electric, hybrid, and fuel-cell vehicles: Architectures and modeling*, IEEE Trans. Veh. Technol. 59 (2010), pp. 589–598.
[2] S. Murata, *Innovation by in-wheel-motor drive unit*, 10th International Symposium on Advanced Vehicle Control (AVEC), Loughborough, UK, 2010.
[3] Y. Hori, *Future vehicle driven by electricity and control – Research on four-wheel-motored UOT electric march II*, IEEE Trans. Ind. Electron. 51 (2004), pp. 954–962.
[4] J. Rauh and D. Ammon, *System dynamics of electrified vehicles: Some facts, thoughts, and challenges*, Veh. Syst. Dyn. 49 (2011), pp. 1005–1020.
[5] G. Yimin, C. Liang, and M. Ehsani, *Design and control principles of hybrid braking system for EV, HEV and FCV*, IEEE Vehicle Power and Propulsion Conference (VPPC), Arlington, TX, USA, 2007.
[6] L. Pinto, S. Aldworth, M. Watkinson, P. Jeary, and M. Franco-Jorge, *Advanced yaw motion control of a hybrid vehicle using twin rear electric motors*, 10th International Symposium on Advanced Vehicle Control (AVEC), Loughborough, UK, 2010.
[7] J. Brembeck, L.M. Ho, A. Schaub, C. Satzger, J. Tobolar, J. Bals, and G. Hirzinger, *ROMO – The robotic electric vehicle*, 22nd International Symposium on Dynamics of Vehicles on Roads and Tracks, Manchester, UK, 2011.
[8] R. de Castro, R.E. Araujo, and D. Freitas, *A single motion chip for multi-motor EV control*, 10th International Symposium on Advanced Vehicle Control (AVEC), Loughborough, UK, 2010.
[9] S. Savaresi and M. Tanelli, *Active Braking Control Systems Design for Vehicles*, Springer, Berlin, 2010.
[10] F. Wang and B. Zhuo, *Regenerative braking strategy for hybrid electric vehicles based on regenerative torque optimization control*, Proc. Inst. Mech. Eng. D, J. Automob. Eng. 222 (2008), pp. 499–513.
[11] M. Bodson, *Evaluation of optimization methods for control allocation*, J. Guid. Control Dyn. 25 (2002), pp. 703–711.
[12] J.H. Plumlee, D.M. Bevly, and A.S. Hodel, *Control allocation in ground vehicles*, Int. J. Veh. Des. 42 (2006), pp. 215–243.
[13] G. Genta and L. Morello, *The Automotive Chassis, Volume 2: System Design*, Springer, Berlin, 2009.
[14] A.T. van Zanten, *Evolution of electronic control systems for improving the vehicle dynamic behavior*, in *Proceedings of the International Symposium on Advanced Vehicle Control (AVEC)*, Hiroshima, Japan, 2002, pp. 7–15.
[15] O. Mokhiamar and M. Abe, *How the four wheels should share forces in an optimum cooperative chassis control*, Control Eng. Pract. 14 (2006), pp. 295–304.
[16] M. Klomp, *Longitudinal force distribution using quadratically constrained linear programming*, Veh. Syst. Dyn. 49 (2011), pp. 1823–1836.
[17] E. Ono, Y. Hattori, Y. Muragishi, and K. Koibuchi, *Vehicle dynamics integrated control for four-wheel-distributed steering and four-wheel-distributed traction/braking systems*, Veh. Syst. Dyn. 44 (2006), pp. 139–151.
[18] S.I. Sakai, H. Sado, and Y. Hori, *Anti-skid control with motor in electric vehicle*, 6th International Workshop on Advanced Motion Control, Nagoya, Japan, 2000.
[19] M. Ehsani, Y. Gao, S.E. Gay, and A. Emadi, *Modern Electric, Hybrid Electric, and Fuel Cell Vehicles: Fundamentals, Theory, and Design*, CRC Press, Boca Raton, FL, 2005.
[20] D.A. Crolla and D. Cao, *The impact of electric and hybrid powertrains on vehicle dynamics and control systems*, 22nd International Symposium on Dynamics of Vehicles on Roads and Tracks, Manchester, UK, 2011.

[21] T.A. Johansen, I. Petersen, J. Kalkkuhl, and J. Ludemann, *Gain-scheduled wheel slip control in automotive brake systems*, IEEE Trans. Control Syst. Technol. 11 (2003), pp. 799–811.
[22] H. Khalil, *Nonlinear Systems*, 3rd ed., Prentice-Hall, Englewood Cliffs, NJ, 2002.
[23] T.D. Gillespie, *Fundamentals of Vehicle Dynamics*, Society of Automotive Engineers, Warrendale, PA, 1992.
[24] U. Kiencke and L. Nielsen, *Automotive Control Systems For Engine, Driveline, and Vehicle*, Springer, Berlin, 2005.
[25] R. de Castro, R.E. Araujo, and D. Freitas, *Optimal linear parameterization for on-line estimation of tire–road friction*, 18th World Congress of the International Federation of Automatic Control (IFAC), Milano, Italy, 2011.
[26] TMPT, *Tyre Model Performance Test*, Data of measurements. Available at http://tmpt.tuwien.ac.at/ (accessed 4 March 2012).
[27] M. Tanelli, L. Piroddi, and S.M. Savaresi, *Real-time identification of tire-road friction conditions*, IET Control Theory Appl. 3 (2009), pp. 891–906.
[28] H.F. Grip, L. Imsland, T.A. Johansen, J.C. Kalkkuhl, and A. Suissa, *Vehicle sideslip estimation*, IEEE Control Syst. Mag. 29 (2009), pp. 36–52.
[29] L.H. Zhao, Z.Y. Liu, and H. Chen, *Design of a nonlinear observer for vehicle velocity estimation and experiments*, IEEE Trans. Control Syst. Technol. 19 (2011), pp. 664–672.
[30] S. Solyom, A. Rantzer, and J. Lüdemann, *Synthesis of a model-based tire slip controller*, Veh. Syst. Dyn. 41 (2004), pp. 475–499.
[31] E. de Vries, A. Fehn, and D. Rixen, *Flatness-based model inverse for feed-forward braking control*, Veh. Syst. Dyn. 48 (2010), pp. 353–372.
[32] S.C. Baslamisli, I.E. Kose, and G. Anlas, *Robust control of anti-lock brake system*, Veh. Syst. Dyn. 45 (2007), pp. 217–232.
[33] J.I. Miller and D. Cebon, *A high performance pneumatic braking system for heavy vehicles*, Veh. Syst. Dyn. 48 (2010), pp. 373–392.
[34] M. Tanelli, C. Vecchio, M. Corno, A. Ferrara, and S.M. Savaresi, *Traction control for ride-by-wire sport motorcycles: A second-order sliding mode approach*, IEEE Trans. Ind. Electron. 56 (2009), pp. 3347–3356.
[35] B.D.O. Anderson and A. Dehghani, *Challenges of adaptive control-past, permanent and future*, Annu. Rev. Control 32 (2008), pp. 123–135.
[36] J.J.E. Slotine and W. Li, *Applied Nonlinear Control*, Prentice-Hall, Englewood Cliffs, NJ, 1991.
[37] O. Harkegard, *Dynamic control allocation using constrained quadratic programming*, J. Guid. Control Dyn. 27 (2004), pp. 1028–1034.
[38] D.G. Luenberger and Y. Ye, *Linear and Nonlinear Programming*, 3rd ed., Springer, Berlin, 2008.
[39] O. Harkegard, *Efficient active set algorithms for solving constrained least squares problems in aircraft control allocation*, Proceedings of the 41st IEEE Conference on Decision and Control, 2002, pp. 1295–1300.
[40] Mechanical Simulation Corporation, CarSim 8.0 User Manual, 2009.
[41] H.B. Pacejka, *Tyre and Vehicle Dynamics*, Butterworth–Heinemann, London, 2002.

Appendix 1. Vehicle and actuator parameters

The values of the vehicle, actuators and controller parameters are defined in Tables A1 and 1.

Table A1. Parameters of the vehicle, actuators and controller employed in the simulations.

Quarter car mass, M (kg)	$\frac{1000}{4}$
Wheel inertia, J (kg m^2)	1.5
Wheel radius, r (m)	0.3
Maximum electric torque, $T_{\mathrm{e,n}}$ (N m)	200
Electric motor nominal speed, ω_{n} (km/h)	50
Maximum torque of the friction brakes, $T_{\mathrm{f,max}}$ (N m)	2000
Time constant of the friction brakes, τ_f (ms)	16
Dead time of the friction brakes, δ_f (ms)	15
Time constant of the electric motor, τ_e (ms)	1.5
Dead time of the electric motor, δ_e (ms)	0.5
Maximum torque variation rate of the friction brakes, $\dot{T}_{\mathrm{f,max}}$ (kN/s)	10
Maximum torque variation rate of the electric motor, $\dot{T}_{\mathrm{e,max}}$ (kN/s)	30
Speed threshold, v_o (km/h)	5
k_v	1
Dead zone, ε	0.005
Controller gain[a], k	222
Adaption rate[a], γ	300,000
Initial estimate, $\boldsymbol{\theta}_N = rF_z[1.22 - 0.45\,0.18 - 1.19 - 0.25]^{\mathrm{T}}$	
Controller sampling time, t_{s} (s)	$\frac{1}{500}$

[a] In the case of electric motor fail, the control parameters are reduced to $k = 88.8$ and $\gamma = 200{,}000$.